Journal of Biomedical Optics

SPIEDigitalLibrary.org/jbo

Microcirculation assessment using an individualized model for diffuse reflectance spectroscopy and conventional laser Doppler flowmetry

Tomas Strömberg
Hanna Karlsson
Ingemar Fredriksson
Fredrik H. Nyström
Marcus Larsson

SPIE

Microcirculation assessment using an individualized model for diffuse reflectance spectroscopy and conventional laser Doppler flowmetry

Tomas Strömberg,[a,*] Hanna Karlsson,[a] Ingemar Fredriksson,[a,b] Fredrik H. Nyström,[c] and Marcus Larsson[a]
[a]Linköping University, University Hospital, Department of Biomedical Engineering, Linköping 581 85, Sweden
[b]Perimed AB, Datavägen 9A, Järfälla 175 43, Sweden
[c]Linköping University, University Hospital, Department of Medical and Health Sciences, Linköping 581 85, Sweden

Abstract. Microvascular assessment would benefit from co-registration of blood flow and hemoglobin oxygenation dynamics during stimulus response tests. We used a fiber-optic probe for simultaneous recording of white light diffuse reflectance (DRS; 475–850 nm) and laser Doppler flowmetry (LDF; 780 nm) spectra at two source-detector distances (0.4 and 1.2 mm). An inverse Monte Carlo algorithm, based on a multiparameter three-layer adaptive skin model, was used for analyzing DRS data. LDF spectra were conventionally processed for perfusion. The system was evaluated on volar forearm recordings of 33 healthy subjects during a 5-min systolic occlusion protocol. The calibration scheme and the optimal adaptive skin model fitted DRS spectra at both distances within 10%. During occlusion, perfusion decreased within 5 s while oxygenation decreased slowly (mean time constant 61 s; dissociation of oxygen from hemoglobin). After occlusion release, perfusion and oxygenation increased within 3 s (inflow of oxygenized blood). The increased perfusion was due to increased blood tissue fraction and speed. The supranormal hemoglobin oxygenation indicates a blood flow in excess of metabolic demands. In conclusion, by integrating DRS and LDF in a fiber-optic probe, a powerful tool for assessment of blood flow and oxygenation in the same microvascular bed has been presented. [DOI: 10.1117/1.JBO.19.5.057002]

Keywords: diffuse reflectance spectroscopy; laser Doppler flowmetry; modeling; Monte Carlo simulations; microcirculation; blood oxygen saturation; skin physiology.

Paper 130874PRR received Dec. 9, 2013; revised manuscript received Apr. 4, 2014; accepted for publication Apr. 7, 2014; published online May 1, 2014.

1 Introduction

The microcirculatory system is important for delivering oxygen to all cells in the body through the red blood cells (RBC). By measuring the blood flow and the local tissue oxygenation at rest and during provocations, an assessment of the microcirculation can be obtained. In diabetic patients, an impaired vascular capacity has been found by measuring the laser Doppler flowmetry (LDF) perfusion during local skin heating to 44°C for 25 min.[1,2] A possible mechanism for the dysfunction in the microcirculation is microangiopathy due to microvascular stenosis.[3] Transcutaneous oxygen measurements (tcpO2) can be used to diagnose peripheral arterial disease, where critical limb ischemia is manifested in a reduced transcutaneous oxygen partial pressure.[4] The postocclusive reactive hyperemia after arterial occlusion can be used to differentiate between peripheral arterial occlusive disease and normals by using separately or combinations of LDF, DRS, tcpO2, or near-infrared (NIR) spectroscopy.[5–8] Despite assessing various aspects of the microcirculation, however, these methods do not measure the same vascular bed.

In conventional LDF, the microvascular perfusion (concentration times average speed of RBC) is calculated based on the detector photocurrent power spectrum. By tissue modeling, absolute speeds (magnitude of velocity) can be estimated.[9] Diffuse reflectance spectroscopy (DRS) can be used for assessing the tissue concentration of various chromophores, such as hemoglobin. Using white light in the visible to NIR wavelength range and small source-detector separations will, due to high tissue scattering, allow for superficial sampling of tissue, which is perfused mainly by the vessels in the microcirculation. In this wavelength range, the absorption spectra of oxygenized and reduced hemoglobin show distinct features, which enable the determination of hemoglobin oxygenation.

To develop a DRS algorithm, a valid light transport model is needed. Inherent in this model is a geometrical simplification of the skin structure of adequate detail.[10,11] For small source-detector separations, diffusion theory fails to accurately describe light propagation. Numerical simulations using Monte Carlo techniques provide a way to overcome this and can be used to accurately model arbitrary complex structures. It has previously been shown that a homogeneous model fails to describe the light propagation in skin at multiple source-detector separations (0.4 and 1.2 mm) in the visible wavelength range.[12] Skin models with up to nine layers have been used for forward modeling of DRS spectra.[13] Wang et al.[14] and Yudovsky et al.[15] used Monte Carlo simulations of a two-layered-tissue model for estimating tissue optical properties (OP). Yudovsky et al. demonstrated that spatial frequency domain reflectance from a two-layered tissue model could be used for estimating dermis absorption and reduced scattering, while the optical thickness could only be determined for the epidermis layer, and that with limited accuracy. Wang et al. used spatially resolved diffuse reflectance and found that upper layer thickness improved upper layer OP

*Address all correspondence to: Tomas Strömberg, E-mail: tomas.stromberg@liu.se

estimation while lower layer OP accuracy deteriorated. These studies determine OP using absolute calibrated reflectance at a single wavelength and can be extended to spectroscopic use.

The approach proposed in this article differs in that it utilizes a subset of Monte Carlo simulated data for a limited number of tissue geometry and scattering parameters while adding the unique absorption characteristics of each chromophore directly in the inverse Monte Carlo algorithm. This is done by applying Beer–Lambert's law on multiple path length distributions in each layer in the forward calculation.[16] Recordings were taken at two source-detector distances to make the method more sensitive to the layered structure of skin. The inverse algorithm was designed to take the ratio between the intensities at the two distances into account, but not the absolute intensity. This eliminates the need for an absolute calibration of the DRS system,[17] which is a significant advantage since absolute calibration is difficult to perform accurately. Hence, the need for a well-characterized calibration phantom that is stable over time is eliminated.

The aim of this paper was to clinically evaluate a fiber-optic probe-based system integrating DRS and LDF. For the DRS recordings, various models based on a three-layered skin geometry were compared. The LDF signals were analyzed in a conventional way. Recordings were done in human forearm skin before, during, and after systolic occlusion, including a 1 min work period to further deplete oxygen in the forearm. By essentially measuring the same vascular bed, the inter-relationships between the absolute concentration of RBC, hemoglobin oxygenation and tissue perfusion, were studied.

2 Models, Materials, and Measurements

2.1 *Three-Layered Skin Model*

Photon propagation in tissue was modeled using Monte Carlo simulations of a three-layered bio-optical model with 10 free parameters. This is a further development of a nine-parameter DRS model,[16] with the addition of a variable wavelength dependence for melanin absorption (δ, see below). The design was based on previously presented models,[10,11] and consisted of one epidermal layer with a variable thickness t_{epi} [mm] and two dermal layers where the upper had a fixed thickness of 0.5 mm and the lower an infinite thickness. The scattering coefficient [mm^{-1}] was equal for all layers and was modeled as a function of α, β, and γ as

$$\mu_{\mathrm{s}}(\lambda) = \alpha[(1-\gamma)(\lambda/\lambda_0)^{-\beta} + \gamma(\lambda/\lambda_0)^{-4}], \tag{1}$$

where λ is the wavelength [nm] and $\lambda_0 = 600$ nm. The epidermis layer contained a fraction of melanin (f_{mel}[-]) where the absorption coefficient [mm^{-1}] of melanin decays with wavelength with the variable exponent β_{mel}, normally between 2 and 5:[18]

$$\mu_{\mathrm{a,mel}}(\lambda) = 6.6 \cdot 10^{10}\lambda^{-\beta_{\mathrm{mel}}}. \tag{2}$$

The absorption coefficient [mm^{-1}] of the epidermis layer was modeled as

$$\mu_{\mathrm{a,epid}}(\lambda) = f_{\mathrm{mel}}\mu_{\mathrm{a,mel}}(\lambda). \tag{3}$$

The dermis layers contained different tissue fractions of blood ($f_{\mathrm{blood},n}$ where n is the dermis layer number) as a function of the average blood tissue fraction of the two layers ($f_{\mathrm{blood,avg}}$) and the relative ratio between the layers ($f_{\mathrm{blood,rel}}$; ranging between -1 and 1). The same blood oxygen saturation was used in both layers (S_{O2}[-]). The absorption coefficient of blood was given by

$$\mu_{\mathrm{a,blood}}(\lambda) = S_{\mathrm{O2}}\mu_{\mathrm{a,oxy}}(\lambda) + (1 - S_{\mathrm{O2}})\mu_{\mathrm{a,deoxy}}(\lambda), \tag{4}$$

based on the absorption spectra of fully oxygenated and deoxygenated blood ($\mu_{a,\mathrm{oxy}}$ and $\mu_{a,\mathrm{deoxy}}$, respectively, hematocrit of 43%).[19] The absorption coefficient of the dermal layers was given by

$$\mu_{\mathrm{a},n}(\lambda) = f_{\mathrm{blood},n}c_{\mathrm{vp}}(\lambda)\mu_{\mathrm{a,blood}}(\lambda), \tag{5}$$

where c_{vp} is a compensation factor for the vessel packaging or pigment packaging effect caused by the inhomogeneous distribution of blood (located in discrete vessels rather than being homogeneously distributed in the layers). This factor depends on the average vessel diameter D [mm] according to[6,14,15]

$$c_{\mathrm{vp}}(\lambda) = \frac{1 - \exp[-D\mu_{\mathrm{a,blood}}(\lambda)]}{D\mu_{\mathrm{a,blood}}(\lambda)}. \tag{6}$$

For more details on calculating the model parameters from the free parameters see Ref. 16. The tissue fraction of RBC (C_{rbc}) was calculated by averaging the RBC tissue fractions in the two layers based on estimation of the sampling volume.

2.2 *Inverse Problem*

The parameters were obtained by solving the least-square problem by fitting model data to measured data using a trust region reflective algorithm. The error function in the optimization problem takes into account the intensity difference between the modeled and measured data (2×32 points) and emphases the shape of the spectra in the hemoglobin wavelength region (12 points). It also penalizes a deviation from unity in the intensity relaxation factor (1 point) and nonphysiological values on the output parameters (4 points).[20] The model fitting was done in three steps.[20] First, an appropriate starting point was found for parameters mostly affecting wavelengths above 700 nm, i.e., the epidermal thickness, the three scattering parameters, the melanin fraction, the melanin exponent, and the average fraction of blood (preliminary). In the second step, the average fraction of blood, the relative ratio between the layers, the oxygen saturation, and the vessel diameter, were obtained by fitting the whole spectra, where the parameter values obtained from step one were used as starting point. The third step included a model fitting of all 10 parameters using the parameters in steps one and two as starting point. Multiple random starting points were used in steps one and two to ensure that the global optimum was found.

2.3 *Testing Parameter Importance*

The spectral fitting of various analysis models including different sets of the 10 parameters was statistically compared by evaluating the χ^2-statistics for the error function. The full analysis model (χ^2_{all}), was compared to the analysis model with a reduced number of parameters, one parameter being fixed at a time: no compensation for the vessel packaging effect ($\chi^2_{D=0}$), constant vessel diameter at 33 μm ($\chi^2_{D=0.033}$), constant epidermis with thicknesses 50 μm ($\chi^2_{t_{\mathrm{epi}}=0.050}$), removing the scattering parameter γ ($\chi^2_{\gamma=0}$), the same RBC tissue fraction in both dermis layers ($\chi^2_{f_{\mathrm{blood,rel}}=0}$) and constant melanin exponents

($\delta = -10/3$). The χ^2-error for the full analysis model versus any of the reduced analysis models was tested using the test variable

$$v = \frac{\chi^2_{\text{red}} - \chi^2_{\text{all}}}{n_{\chi^2_{\text{all}}} - n_{\chi^2_{\text{red}}}} \Big/ \frac{\chi^2_{\text{all}}}{N - n_{\chi^2_{\text{all}}} - 1}, \quad (7)$$

where χ^2_{red} is any of the reduced analysis models, n is the number of parameters in the given analysis model (10 for the full model, 9 for all the reduced models), and N is the number of points in the χ^2 statistics ($32 \times 2 + 12 + 1 = 77$, 4 nonphysiological outputs omitted). The test variable v is $F(1, N - n_{\chi^2_{\text{all}}} - 1) = F(1, 66)$ distributed. A $v > 7.04$ indicates that the full model has a significantly lower χ^2-error than the reduced model at a level of significance of $p < 0.01$. This test comparing residual spectra for different models is described elsewhere.[21]

2.4 *In Vivo Measurements*

2.4.1 *Subjects and protocol*

Measurements were performed in the supine posture on the volar forearm of 33 healthy participants (9M, 24F) after an acclimatization and resting period of 15 min. The subjects had a mean systolic blood pressure (SBP) of 110 mm Hg (SD = 11) and a mean diastolic blood pressure (DBP) of 68 mm Hg (SD = 8), and one of the subjects was taking angiotensin-converting enzyme (ACE) inhibitors. The mean age for the subjects was 35 years (SD = 9) and the measurements were conducted in a room with an ambient temperature of 22.9 °C (SD = 0.5). The participants had, during 90 days before the measurements, either consumed 150 ml of red wine/day for women or double the amount for men, or been in total alcohol abstention in a larger randomized study evaluating the nonacute effects of alcohol intake on cardiovascular risk factors.[22] This, however, turned out to have no significant effect on the microcirculatory results presented in this study. The measurements were done nonfasting during daytime after at least 12 h since alcohol intake in the wine consuming group. The participants were asked to refrain from coffee/caffeine and smoking the day of the measurements. Of all 33 participants, 16 subjects had been consuming red wine and 17 subjects had been in the alcohol abstention group.

The protocol involved a recording of 1 min baseline, 5 min systolic occlusion to 30 mm Hg above the individual systolic pressure, using a brachial pressure cuff, release of the occlusion, and 5-min postocclusion. The subjects were asked to work the arm by squeezing a ball repeatedly during the fourth minute into the systolic occlusion.

The study was approved by the Regional Ethics Committee of Linköping (D.nr M246-08) and written informed consent was obtained from all participants.

2.4.2 *Hardware*

A custom-made optical fiber probe was used to deliver light to the tissue and to transmit the backscattered light to the detectors. The DRS and LDF illuminating fibers were placed near the center of the probe tip (light sources: Avalight-HAL-S, Avantes BV, The Netherlands, and a diode laser at 780 nm, respectively). Two DRS light collecting fibers were placed at 0.4 and 1.2 mm away from the center of the illuminating fiber and connected to a two-channel spectroscope (475–850 nm; AvaSpec 2048-5 RM, Avantes BV, The Netherlands). One LDF light collecting fiber was placed 0.4 mm from the light emitting fiber. A Periflux 5000 (Perimed AB, Järfälla, Sweden; modified for 50-kHz digital recording of the detected signals; time varying part ac; static light intensity dc), was used for data collection. The fibers were made of fused silica, had a diameter of 200 μm and a numerical aperture of 0.37. The measurement probe was placed in a plastic probe holder (PH 08; Perimed AB, Järfälla, Sweden), which was fixated to the skin using double-sided adhesive rings (PF 105-1; Perimed AB). This assured a minimum contact pressure between the probe tip and the examined skin.

2.4.3 *Signal processing*

The LDF perfusion, *Perf*, was conventionally calculated, using digital signal processing of the time varying ac signal and the light intensity dc signal.[23]

The DRS spectra for the two source-detector separations were preprocessed in three calibration steps:

1. A dark spectrum, recorded before each measurement on a subject, was subtracted.
2. The spectrum was normalized with a white reference spectrum, recorded from a barium sulfate covered surface.
3. The spectrum at each source-detector separation was normalized by the mean intensity at 612–617 nm (mean over wavelength and source-detector distances) from a measurement (calibrated according to steps 1 and 2 above), where the face of the probe was evenly illuminated.

Steps 2 and 3 are both relative calibration steps that enable interwavelength and interchannel intensity comparisons. No additional calibration between modeled and measured intensity is necessary as this difference is removed when solving the inverse problem by normalizing with their average intensity [Eq. (24) in Ref. 16]. By introducing an intensity relaxation factor in the optimization algorithm, the measured relative intensity between the two DRS detectors is allowed to deviate slightly from the modeled.

Spectrometer drift was assessed by comparing recordings from an intensity reference that was obtained before and after each occlusion provocation. The ratios of the intensity after/before for each of the two DRS channels were analyzed. If the mean ratio was >10% (in the wavelength intervals 450–760 and 820–850 nm) or if there was a color change >10% [abs(max ratio – min ratio)] data from that subject were excluded.

DRS spectra were averaged for 1 s and similarly for *Perf*. DRS and LDF data were calculated as the mean value over 45 s for baseline and as the mean value over 10 s for prework and prerelease, respectively. Data after release were calculated from an average spectrum over 1 s for DRS.

The time constants for S_{O2} and *Perf* during occlusion and release were calculated based on the parameter values at baseline and before arm work, and the parameter values after work and after release, respectively. The time constants were calculated as the time differences between 75% and 25% of those values.

3 Results

3.1 *Data Exclusion*

Data from eight subjects were excluded due to spectrometer drift. Data from three subjects were excluded due to inadequate

hyperemia (<15 s duration of increased *Perf* after release of occlusion, compared to baseline). The mean age of the remaining subjects (17F, 5M) was 35 (SD = 9) years, mean SBP was 110 mm Hg (SD = 12) and mean DBP was 69 mm Hg (SD = 9). None of the remaining subjects were taking any blood pressure medication. The mean room temperature was 22.9 (SD = 0.5)°C.

3.2 *Model Choice*

The spectral fitting for the reduced models was compared to the full model at baseline and after release of occlusion (Table 1). The results show that γ, $f_{\text{blood,rel}}$ and β_{mel} cannot be removed from the model, and are in favor of keeping D and t_{epi} in the model. Hence, we chose to keep the full model for the subsequent analysis.

An example of the DRS spectral fitting is given in Fig. 1 at baseline and after occlusion release. Note the lower intensity in the 470–570 nm range, where hemoglobin absorption spectra have characteristic peaks, after occlusion release. The residual spectra are within 10% and show no systematic shape. The good spectral fit is enabled by including the intensity relaxation factor, which eliminates deviations between the intensity ratios between the two source-detector distances. The model was within 10% at both source-detector distances for all spectra and all wavelengths.

Table 1 Number of spectra ($N = 22$ subjects) at baseline/after occlusion release where the full model is significantly better than the reduced model.

Reduced model	No. of spectra
$D = 0$	13/17
$D = 0.033$	5/8
$t_{\text{epi}} = 0.050$	8/8
$\gamma = 0$	20/18
$f_{\text{blood,rel}} = 0$	17/18
$\beta_{\text{mel}} = -10/3$	10/11

3.3 *Test of Wine Effect*

Out of 22 subjects, 10 consumed wine (7F, 3M) and 12 refrained from alcohol (10F, 2M). The parameters S_{O2}, C_{rbc}, and *Perf* were compared between the two groups at baseline and after release of occlusion using the Mann-Whitney U-test (nonparametric test due to significantly different variances between the groups). No significant differences were found between the groups in any parameter. Data from the two groups were, therefore, pooled in the subsequent analysis.

3.4 *Full Model Data*

Spectral fitting ([model – measured]/model), when compensating for the intensity difference between the two distances (the intensity relaxation factor),[24] was calculated for one spectrum per phase (baseline, prework, prerelease, and after release). The individual mean (SD) intensity relaxation factor was 0.81 (0.15); 0.80 (0.16); 0.79 (0.15); 0.79 (0.16), at these time points, respectively.

The output data for a typical recording are presented in Fig. 2. The occlusion, starting at $t = 65$ sm causes a sudden drop in *Perf*, a slower drop in S_{O2} to almost zero, and a slower increase in C_{rbc} due to venous filling before occlusion pressure is above systolic. During the forearm work period (250–310 s), *Perf* increased due to motion artifacts. After release (365 s), a reactive hyperemia is observed with a *Perf* increase to values above baseline during 78 s, associated with a persistent increase in S_{O2}.

Mean data for the output variables during the occlusion procedure are given in Table 2. There was a significant difference between the phases for all parameters ($p < 0.001$, Friedman ANOVA by ranks). The occlusion (prework and prerelease versus baseline) caused S_{O2} and *Perf* to drop, while C_{rbc} increased. After release S_{O2}, *Perf* and C_{rbc} were higher than at baseline. The relative increase in *Perf* (after release versus baseline) was 373 (212)%, while the relative increase in C_{rbc} was 93 (39)%. This indicates that the major part of the increase in *Perf* was due to an increased average speed of the RBCs.

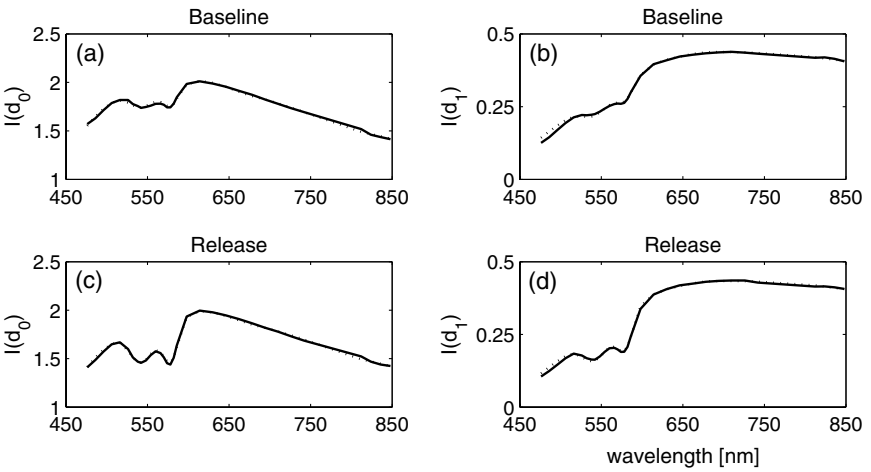

Fig. 1 Measured (solid) and full model (dotted) DRS spectra (I = intensity), recorded at the source detector distances $d_0 = 0.4$ mm (a, c) and $d_1 = 1.2$ mm (b, d) for subject #18 at baseline (a, b) and after occlusion release (c, d).

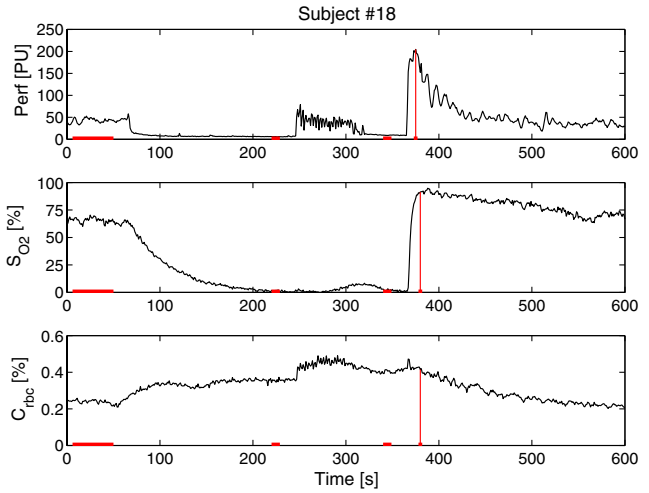

Fig. 2 Time resolved *Perf* from LDF, S_{O2} and C_{rbc} from DRS for subject #18). Time points for baseline (45 s), prework, prerelease (10 s each) are marked with a horizontal line (light gray/ red). Values at release (1 s) are marked with a vertical line (light gray/ red).

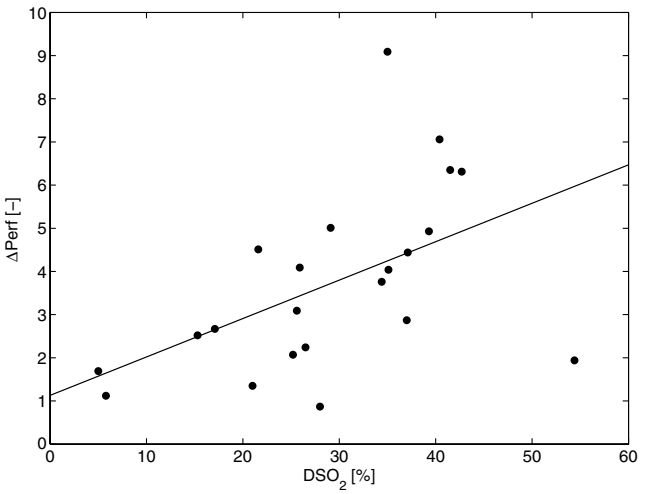

Fig. 3 Relative change in perfusion ($\Delta Perf$) and absolute changes in oxygenation (DS_{O2}; % units), comparing after occlusion release and baseline.

The time constant (75% to 25% and 25% to 75%), for the S_{O2} decay during occlusion, was 61 (21) s and the time constant during the release was 2 (5) s. The corresponding time constants for *Perf* were difficult to calculate for several individuals due to motion artifacts during occlusion. In general, however, the time constants during occlusion were below 10 s and during release below 2 s.

There was a significant relationship between relative changes in *Perf* (release/baseline − 1) and absolute changes in S_{O2} (release − baseline; $p < 0.05$ Fig. 3). There was no such relationship between the changes in *Perf* and the changes in C_{rbc}, nor between the changes in S_{O2} and the changes in C_{rbc}. These findings indicate that the increase in *Perf* is due to high velocity blood flow, either in the capillaries or in the larger feeding vessels.

4 Discussion

In summary, we have presented a method for measuring blood flow and tissue oxygenation in the same vascular bed using a fiber-optic probe integrating DRS and LDF. DRS data were analyzed using an individually adaptive tissue model. An optimal choice of parameters in the skin model was determined. This together with a new calibration scheme allowed DRS spectra modeling at two source-detector separations within 10%. Output data of S_{O2}, C_{rbc}, and *Perf* were calculated during a protocol involving 5-min systolic occlusion. During occlusion, *Perf* decreased rapidly, while S_{O2} was lowered slowly, and C_{rbc} increased slowly. During occlusion release, a rapid hyperemic response was observed with supranormal *Perf* and S_{O2}. The increase in *Perf* was due to an increase in both blood tissue fraction and speed. Before discussing the clinical findings in detail, some methodological issues will be considered.

The evaluation of various light transport models with a reduced number of parameters was conclusive regarding the importance of having γ, $f_{blood,rel}$ and β_{mel} in the model, while the results regarding D and t_{epi} were less clear. The γ and β_{mel} are important for a more detailed modeling above 700 nm where light scattering in tissue and the melanin light absorption foremost affect the spectra. The $f_{blood,rel}$ and t_{epi} are important for adapting the relative amount of light in the 500–600 nm region between the two DRS detecting fibers, where hemoglobin has predominant light absorption. We have previously concluded that a homogenous tissue model cannot be used to model DRS spectra at two source-detector distances.[12,16]

The findings of an intensity relaxation factor between the two distances of 0.8 as an average deviate from results on tissue phantoms, where a ±10% tolerance was able to model data.[24] The deviation from unity in the ideal case could possibly be due to differences in surface contact with the skin in this study as compared to the optical liquid phantoms. Another effect may be due to differences in the spectral color due to spectrometer drift that was not compensated for. It can also be due to the limited ability of the three-layered model to mimic the skin.

The effect of wine consumption on the microcirculation was tested by comparing the parameters S_{O2}, C_{rbc}, and *Perf* at

Table 2 DRS tissue model parameters and LDF *Perf* during various phases of the recording: oxygen saturation (S_{O2}), tissue fraction of red blood cells (C_{rbc}). Wilcoxon's matched pairs test.

	Baseline	Prework	Prerelease	Release
S_{O2} [%]	46 (12)	5.6 (7.3) ***	11 (12)***	75 (13) ***
C_{rbc} [%]	0.20 (0.074)	0.34 (0.11) ***	0.46 (0.22) ***	0.38 (0.13) ***
Perf [PU]	37 (22)	10 (7.1) ***	18 (16) ***	148 (56) ***

Note: Statistical comparison with baseline, *** $p < 0.001$.

baseline and after release of occlusion. No significant differences were found between the groups in any parameter. The effect of alcohol on liver fat and blood lipids was studied in the larger study group ($N = 44$) from which we recruited our subjects. A borderline significant trend of increased liver fat and a decrease in LDL cholesterol was observed in wine consumers.[22] We found no significant statistical difference between the groups regarding the microcirculatory parameters. These results support the adequacy of pooling data from wine consumers and those that refrained from alcohol in this study. However, due to the small sample size, we cannot rule out a possible minor microcirculatory effect of wine consumption. As for the study protocol, an occlusion to a pressure of 30 mm Hg above the individual systolic pressure, in some cases caused only a mild hyperemic response. This protocol has been used before,[5] although others use a pressure at 200 mm Hg, which in normotensive subjects is much more than 30 mm Hg above the systolic pressure. Our data indicate that a pressure of 200 mm Hg is preferable in normal subjects.

The combination of LDF and DRS assessing the same vascular bed gives new possibilities to interpret physiological reactions. One example is the slow (mean time constant 61 s; Fig. 2) decrease in S_{O2} during occlusion by diffusion of oxygen to the tissue, while the increase in S_{O2} during occlusion release is a flow process, which is much faster (mean time constant 2 s). This is confirmed by simultaneous *Perf* recordings using LDF. As for the vascular complexes involved in the hyperemic phase, the overshoot in S_{O2} is due to a vasodilation since C_{rbc} is increased. However, this vasodilation is not uniform in the vascular tree, since the RBC would then have the same average speed. However, the increase in *Perf* is higher than in C_{rbc}, indicating an increased average RBC speed. Therefore, we assume that the vasodilation is predominant in larger vessels with a higher average RBC speed.

A further development of the method presented in this study is to integrate the DRS and LDF modalities in a fully model-based analysis where also the LDF spectra are fitted to a model.[11,16,20] Some of the difficulties in the clinical interpretation of which vascular beds that underlie the results may be overcome by the differentiation of LDF perfusion into different speed components.[11]

In conclusion, simultaneous measurements of *Perf*, S_{O2} and C_{rbc} in the microcirculation enable a more detailed physiological assessment of local tissue vascular status. A model-based speed-resolved LDF perfusion will further enhance the method. However, much effort remains in the fine tuning of the optimal interpretation schemes.

Acknowledgments

The study was financed by VINNOVA and Perimed AB through the SamBIO research collaboration program between companies and academia within bioscience (VINNOVA D. No. 2008-00149), through the Research and grow programme (VINNOVA D. No. 2011-03074), and also by NovaMedTech, supported by the European Union Regional Development Fund.

References

1. I. Fredriksson et al., "Reduced arterio-venous shunting capacity after local heating and redistribution of baseline skin blood flow in type 2 diabetes assessed with velocity-resolved quantitative laser Doppler flowmetry," *Diabetes* **59**(7), 1578–1584 (2010).
2. G. Rayman et al., "Impaired microvascular hyperaemic response to minor skin trauma in type I diabetes," *Br. Med. J.* **292**(6531), 1295–1298 (1986).
3. J. E. Tooke, "Perspectives in diabetes. Microvascular function in human diabetes. A physiological perspective," *Diabetes* **44**, 721–726 (1995).
4. L. Norgren et al., "Inter-society consensus for the management of peripheral arterial disease (TASC II)," *J. Vasc. Surg.* **45** S5–67 (2007).
5. F. Morales et al., "How to assess post-occlusive reactive hyperaemia by means of laser Doppler perfusion monitoring: application of a standardised protocol to patients with peripheral arterial obstructive disease," *Microvasc. Res.* **69**, 17–23 (2005).
6. R. Kragelj et al., "Parameters of postocclusive reactive hyperemia measured by near infrared spectroscopy in patients with peripheral vascular disease and in healthy volunteers," *Ann. Biomed. Eng.* **29**, 311–320 (2001).
7. X. Cheng et al., "Post-occlusive reactive hyperemia in patients with peripheral vascular disease," *Clin. Hemorheol. Microcirc.* **31**(1), 11–21 (2004).
8. G. Zonios, J. Bykowski, and N. Kollias, "Skin melanin, hemoglobin, and light scattering properties can be quantitatively assessed in vivo using diffuse reflectance spectroscopy," *J. Invest. Dermatol.* **117**, 1452–1457 (2001).
9. M. Larsson and N. Strömberg, "Toward a velocity-resolved microvascular blood flow measure by decomposition of the laser Doppler spectrum," *J. Biomed. Opt.* **11**(1), 014024 (2006).
10. I. Fredriksson, M. Larsson, and T. Strömberg, "optical microcirculatory skin model: assessed by Monte Carlo simulations paired with in vivo laser Doppler flowmetry," *J. Biomed. Opt.* **13**(1), 014015 (2008).
11. I. Fredriksson, M. Larsson, and T. Strömberg, "Quantitative laser Doppler flowmetry in skin," *J. Biomed. Opt.* **15**(5), 057002 (2010).
12. H. Karlsson et al., "Can a one-layer optical skin model including melanin and inhomogenously distributed blood explain spatially resolved diffuse reflectance spectra?," *Proc. SPIE* **7896**, 78962Y (2011).
13. T. Maeda et al., "Monte Carlo simulation of spectral reflectance using a multilayered skin tissue model," *Opt. Rev.* **17**(3), 223–229 (2010).
14. Q. Wang, K. Shastri, and T. J. Pfefer, "Experimental and theoretical evaluation of a fiber-optic approach for optical property measurement in layered epithelial tissue," *Appl. Opt.* **49**(28), 5309–5320 (2010).
15. D. Yudovsky and A. J. Durkin, "Spatial frequency domain spectroscopy of two layer media," *J. Biomed. Opt.* **16**(10), 107005 (2011).
16. I. Fredriksson, M. Larsson, and T. Strömberg, "Inverse Monte Carlo method in a multilayered tissue model for diffuse reflectance spectroscopy," *J. Biomed. Opt.* **17**(4), 047004 (2012).
17. P. R. Bargo et al., "In vivo determination of optical properties of normal and tumor tissue with white light reflectance and an empirical light transport model during endoscopy," *J. Biomed. Opt.* **10**(3), 034018 (2005).
18. S. L. Jacques, "Optical properties of biological tissues: a review," *Phys. Med. Biol.* **58**(11), R37 (2013).
19. W. G. Zijlstra, A. Buursma, and O. W. van Assendelft, *Visible and Near Infrared Absorption Spectra of Human and Animal Haemoglobin Determination and Application*, VSP Books, Utrecht, Boston, Köln, Tokyo (2000).
20. I. Fredriksson et al., "Inverse Monte Carlo in a multilayered tissue model–merging diffuse eflectance spectroscopy and laser Doppler flowmetry," *J. Biomed. Opt.* **18**(12), 127004 (2013).
21. D. G. Kleinbaum, "Selecting the best regression equation," in *Applied Regression Analysis and Other Multivariable Methods*, Belmont, Ed., Brooks/Cole, California (2008).
22. S. Kechagias et al., "Effects of moderate red wine consumption on liver fat and blood lipids: a prospective randomized study.," *Annals. Med.* **43** 545–554 (2011).
23. M. Larsson, W. Steenbergen, and T. Strömberg, "Influence of optical properties and fibre separation on laser Doppler flowmetry," *J. Biomed. Opt.* **7**(2), 236–243 (2002).
24. H. Karlsson et al., "Inverse Monte Carlo for estimation of scattering and absorption in liquid optical phantoms," *Opt. Express* **20**(11), 12233–46 (2012).

Biographies for the authors are not available.